EARLY SCIENCE WITH THE KOREAN VLBI NETWORK: THE QCAL-1 43 GHz CALIBRATOR SURVEY

Leonid Petrov[1], Sang-Sung Lee[2], Jongsoo Kim[2], Taehyun Jung[2], Junghwan Oh[2,3], Bong Won Sohn[2,3],
Do-Young Byun[2,3], Moon-Hee Chung[2], Do-Heung Je[2], Seog-Oh Wi[2], Min-Gyu Song[2], Jiman Kang[2],
Seog-Tae Han[2,3], Jung-Won Lee[2], Bong Gyu Kim[2,3], Hyunsoo Chung[2], and Hyun-Goo Kim[2]

[1] Astrogeo Center, Falls Church, VA 22043, USA
[2] Korean VLBI Network, Korea Astronomy and Space Science Institute, 776, Daedeokdae-ro, Yuseong-gu, Daejeon 305-348, Republic of Korea; sslee@kasi.re.kr
[3] Yonsei University Observatory, Yonsei University, Seongsan-ro 50, Yonsei-ro, Seodaemun-gu, Seoul 120-749, Republic of Korea

ABSTRACT

This paper presents the catalog of correlated flux densities in three ranges of baseline projection lengths of 637 sources from a 43 GHz (*Q* band) survey observed with the Korean VLBI Network. Of them, 14 objects used as calibrators were previously observed, but 623 sources have not been observed before in the *Q* band with very long baseline interferometry (VLBI). The goal of this work in the early science phase of the new VLBI array is twofold: to evaluate the performance of the new instrument that operates in a frequency range of 22–129 GHz and to build a list of objects that can be used as targets and as calibrators. We have observed the list of 799 target sources with declinations down to $-40°$. Among them, 724 were observed before with VLBI at 22 GHz and had correlated flux densities greater than 200 mJy. The overall detection rate is 78%. The detection limit, defined as the minimum flux density for a source to be detected with 90% probability in a single observation, was in the range of 115–180 mJy depending on declination. However, some sources as weak as 70 mJy have been detected. Of 623 detected sources, 33 objects are detected for the first time in VLBI mode. We determined their coordinates with a median formal uncertainty of 20 mas. The results of this work set the basis for future efforts to build the complete flux-limited sample of extragalactic sources at frequencies of 22 GHz and higher at 3/4 of the celestial sphere.

Key words: astrometry – galaxies: active – radio continuum: galaxies – surveys – techniques: interferometric

Online-only material: color figures, machine-readable and VO tables

1. INTRODUCTION

The Korean VLBI Network (KVN) is the first dedicated very long baseline interferometry (VLBI) network in East Asia in millimeter wavelengths. The KVN was built by Korea Astronomy and Space Science Institute (KASI) in order to achieve the following major goals: (1) to study the formation and death of stars with observing water (H_2O), methanol (CH_3OH), and silicon monoxide (SiO) masers at high resolutions; (2) to investigate the structure and dynamics of our own Galaxy by conducting highly accurate astrometric VLBI observations of Galactic radio sources; and (3) to study the nature of active galactic nuclei (AGNs) and their population at high frequencies. KVN as a dedicated VLBI network also aims to study the spectral and temporal properties of transient sources such as bursting star-forming regions, intraday variable compact radio sources, gamma-ray flaring AGNs, and other objects by conducting systematic multi-wavelength monitoring campaigns (Kim et al. 2004; Lee et al. 2011)

KVN consists of three 21 m radio telescopes: in Seoul, the KVN Yonsei Radio Telescope (KVNYS); in Ulsan, the KVN Ulsan Radio Telescope (KVNUS); and on Jeju island, Korea, the KVN Tamna Radio Telescope (KVNTN). The baseline lengths are in range of 305–476 km (see Figure 1). All antennas have an identical design. The aggregate rms deviation of the antenna surface from a paraboloid is 0.12 mm, which allows us to observe at frequencies of up to 150 GHz. The antennas are equipped with a quasi-optic system that allows simultaneous observations at 22, 43, 86, and 129 GHz. This system is described in detail in Han et al. (2008).

By 2011, the 22 and 43 GHz receivers were installed and carefully tested. The dual beams at two frequencies are well aligned within 5″. The pointing errors are less than 3″ in azimuth and elevation. The measured aperture efficiencies are greater than 64% at 22 GHz and greater than 62% at 43 GHz. More detailed results of performance tests of the antenna and receivers in the single-dish mode are presented in Lee et al. (2011). Receivers at 86 and 129 GHz will be tested in 2012.

The signals digitized by the samplers in the receiver room are processed by the KVN Data Acquisition System (DAS) to obtain spectra for single-dish spectroscopy observations. In VLBI operation, the digitized signals processed in the DAS are recorded onto disks using Mark-5B. In 2011, the aggregate recording rate was limited by 1024 Mbps, which can be used either entirely for one band or split between bands.

KASI has all hardware and software to support *the full cycle of VLBI observations* either as a three-element interferometer or as a part of a larger VLBI network: scheduling, antenna control system, data recording, correlation, post-correlation data processing, astrometry, geodesy, and imaging analysis. First, fringes between KVN stations at 22 GHz in a recording rate of 1 Gbps were obtained on 2010 June 8. Test observations on 2010 September 30 confirmed that the VLBI system works according to specifications. Detailed analysis of system performance will be given in J. A. Lee et al. (in preparation).

These first tests allowed us to start an early science program including multi-frequency phase referencing observations. The feasibility of the multi-frequency phase referencing observations strongly depends on the information about phase calibrators such as their structures, flux densities, global distribution, etc. (Jung et al. 2011). Therefore, it is necessary to establish a catalog of radio compact sources at high frequency bands with large VLBI surveys. This determined our choice for the first early science project for VLBI observations in continuum mode.
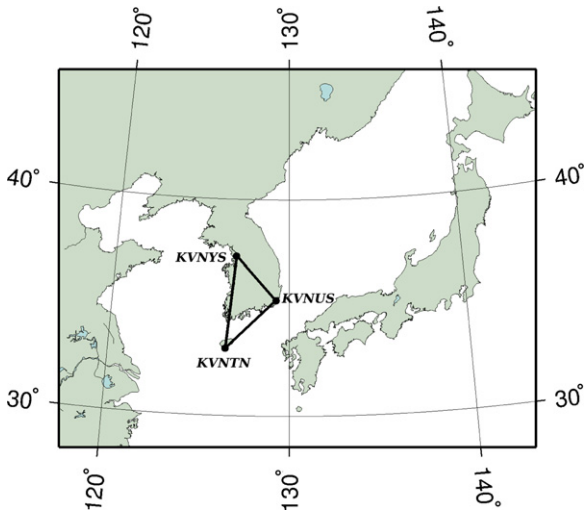
Figure 1. Korean VLBI network.
(A color version of this figure is available in the online journal.)

In this paper, we present results of the 43 GHz VLBI survey conducted at the three-element KVN radio interferometer. We describe the strategy for source selection, observations, and data analysis and present the catalog of correlated flux densities. Finally, we summarize the main findings and make conclusions about the performance of the KVN for AGN studies.

2. THE QCAL-1 SURVEY: GOALS AND SOURCE SELECTION

Although the accumulative radio fundamental catalog[4] (L. Petrov & Y. Kovalev 2013, in preparation) that includes all the sources observed with VLBI in a survey mode as of 2012 August has 7216 objects, the majority of them were observed at frequencies 8 GHz and lower. This catalog is based on Very Long Baseline Array (VLBA) Calibrator Survey (Beasley et al. 2002; Fomalont et al. 2003; Petrov et al. 2005, 2006; Kovalev et al. 2007; Petrov et al. 2007b) and other large surveys. There were only several VLBI surveys at frequencies higher than 24 GHz. Lanyi et al. (2010) observed 132 sources in the Q band in 2002–2003, Marscher et al. (2012) as run an ongoing project of monitoring 34 AGNs since 2007, and Jacobs & Sovers (2009) started to work on the catalog of ~ 300 objects at 32 GHz that will become available in the future. Considering that 13 sources overlap in both projects, the total number of sources with known Q-band flux densities at milliarcsecond scales with their brightness distributions publicly available is 153. This count does not include individual sources that were observed as targets under other programs. All these sources have correlated flux density at baselines longer than 900 km, which corresponds to 130 megawavelengths, greater than 200 mJy.

We would like to increase this list for two reasons. First, we need to have a set of sources suitable as calibrators for high frequencies with KVN and VERA (VLBI Exploration of Radio Astrometry). Observations with quick switching between a weak target and a bright calibrator allow us to extend the coherence time from several minutes to hours, provided a calibrator located within several degrees from a target can be detected. Second, construction of a flux-limited sample of sources at high frequencies provides an opportunity to study the population of AGNs. At frequencies of 43 GHz and higher the

radio emission at parsec scales is dominated by the core. VLBI observations of a large flux-limited sample allow us to derive a number of interesting statistics. In particular, using such a sample we can

1. investigate compactness determined as a ratio of the correlated flux density at short and long baselines to the single-dish flux density and compare it with compactness at 2.2, 8.4, and 22 GHz;
2. measure the brightness temperature for the core and jet components in order to populate a model of the distribution of the observed core brightness temperature in terms of the intrinsic properties of relativistic jets such as the brightness temperature, bulk motion, and viewing angle; the data will also provide the unbiased sample needed to investigate the unified scheme between quasars, BL Lac objects, and galaxies;
3. analyze the relationship between the core optical depth as measured by the spectral index and other properties of the jet emission and optical properties; and
4. investigate the variation of the spectral index along the presumably optically thin jets and comparison with the conditions in small-scale and larger-scale jets.

To commence building a large sample of compact sources at 43 GHz, we analyzed prior VLBI surveys at 22–24 GHz: the K/Q VLBA survey (Lanyi et al. 2010), the VERA 22 GHz fringe search survey (Petrov et al. 2007a), the VLBA Galactic Plane Survey (Petrov et al. 2011), the EVN Galactic Plane Survey (Petrov 2012), and the VERA K-band Calibrator Survey (Petrov at al. 2012). We selected 878 sources in these surveys that have correlated flux densities at scales less than 10 mas exceeding 200 mJy. After subtracting 153 sources that have already been observed in Q-band surveys, we obtained the list of 725 target sources. We added to this list two samples of the sources that were not previously observed with VLBI which we could reasonably expect to be bright enough for being detected in the Q band with KVN. These additional sources included 49 objects from the CGRaBS catalog (Healey et al. 2008), many of them are part of the OVRO 40 m telescope monitoring program at 15 GHz (Richards et al. 2011) (1576 other objects have already been observed with VLBI) and 26 sources from the AT20G catalog (Murphy et al. 2010) with spectral index ($S \sim f^\alpha$) greater than +0.5 that have the flux density extrapolated to 43 GHz greater than 200 mJy. In total, the list of targets included 799 objects.

2.1. Observations

We observed target sources in three observing sessions in 2011 December 18, 19, and 22. The first two sessions had durations 28 and 27 hr, respectively. In the 50 minute long third session, we observed the sources missed in the first two sessions. Each source was scheduled in one scan, 90 s long, in the first observing session and in one scan in the second observing session. The algorithm for automatic scheduling implemented in the software sur_sked[5] selected the sources in a sequence that minimizes slewing.

In addition to target sources, every half an hour a source from the list of 34 blazars that are regularly monitored by the Boston group (Jorstad et al. 2005; Marscher et al. 2012) was inserted. The scheduling algorithm has picked up 14 blazars. These bright

---

Table 1
Dependence of Gain at 43 GHz for KVN Antennas Measured
in 2011 February–March

Station	DPFU	A_0	A_1	A_2
KVNTN	0.0747	0.979990	1.23772×10^{-3}	-1.91393×10^{-5}
KVNUS	0.0714	0.974197	1.41639×10^{-3}	-1.94371×10^{-5}
KVNYS	0.0850	0.923354	3.47852×10^{-3}	-3.94673×10^{-5}

Notes. Gain in Jy K^{-1} is expressed as DPFU $\cdot (A_0 + A_1 \cdot e + A_2 \cdot e^2)$, where e is elevation in degrees.

Table 2
Average Receiver Temperature, Opacity, the System Equivalent Flux Densities
(SEFDs) in Zenith Direction, and A Posteriori Multiplicative Gain Corrections
During the Campaign

Station	T_{rec} (K)	η	β	SEFD (Jy)	Gain$_{corr}$
KVNTN	89	0.945	0.081	2080	1.10
KVNUS	51	0.925	0.082	1460	1.06
KVNYS	103	0.945	0.103	2810	1.31

Notes. Although receiver design for all three stations is identical, the thermal isolator of the Ulsan Q-band receiver is different and it contributes to a significant reduction of receiver temperature. Upgrade of thermal isolators at KVNYS and KVNTN is planned in near future.

sources were used for bandpass calibration and for evaluation of station-dependent gain corrections.

Every hour a tipping curve was measured: each antenna recorded system temperature at eight different elevations. These measurements allow us to monitor changes in the opacity of the atmosphere.

The left circular polarization data were recorded using Mark-5B units with two-bit sampling within the 496 MHz wide band in a range of 42.850–43.346 GHz in 16 intermediate sub-bands of 16 MHz wide, equally spaced in steps of 16 MHz using a digital filter. The aggregate recording rate was 1024 Mbps.

3. DATA ANALYSIS

The data were correlated with DiFX-2 correlator (Deller et al. 2011) with spectral resolution of 0.125 MHz and accumulation periods of one second long. The scheme of post-correlator data analysis was similar to the analysis of the KCAL VERA calibrator survey at 22 GHz (Petrov at al. 2012). First, for each observation we found phase delay rates, group delays, and group delay rates such that, after coherent averaging of complex cross-correlation samples rotated according to these parameters, the fringe amplitude of the sum reached the maxima. We used the analysis software $\mathcal{PIMA}$[6] for performing this task. We call an observation a data set that originates from processing data of one scan at one baseline.

Analyzing the distribution of achieved signal-to-noise ratios (S/Ns), we found the probability of false detection for observations with no signal, but only noise is less than 0.01 when the S/N is greater than 5.4. We used this value of the S/N as a threshold for a preliminary screening of detected and non-detected observations.

Then total group delays and delay rates as well as some auxiliary information were written into a database for further processing with the VTD/post-Solve software[7] for analysis of absolute astrometry and geodesy observations. We solved for coordinates of new sources, baseline lengths, clock function, and residual atmosphere path delay in the zenith direction modeled with a linear B-spline with spans of one hour for every station. This was done for two reasons. First, we were able to adjust the positions of new sources and improve a priori baseline lengths. Second, considering that for a majority of sources their positions are known at a milliarcsecond level, we can make an additional test whether a given source was detected. The group delay search window was 8 μs. If a source is not detected, its estimate of group delay will be uniformly distributed in a range of ± 4 μs. The distribution of post-fit residuals of detected sources has the weighted rms (wrms) 55–80 ps. That is why a non-detected source will show up as an outlier. The probability that a non-detected source whose position is not adjusted will accidentally

have the post-fit residual greater than five times wrms, i.e., ± 0.4 ns, and therefore will not be marked as an outlier, is 10^{-4}.

After additional screening for non-detections by analyzing residuals of parameter estimation and elimination of observations with residuals exceeding five times their wrms, we performed the amplitude calibration. Previous measurements of antenna gains showed that they vary with elevation within 5%–8%. Table 1 provides parameters of gains used in our analysis.

Analysis of system temperature measurements revealed small variations with time and with elevation angle. The measured system temperature is considered as a sum of three terms: the receiver temperature T_{rec}, the spillover temperature T_{spill}, and the contribution of the atmosphere:

$$T_{sys} = T_{rec} + \eta\, T_{atm}[1 - e^{-\beta\, m(e)}] + (1 - \eta)T_{spill}, \quad (1)$$

where T_{atm} is the average temperature of the atmosphere; β is the atmosphere opacity; η is the spillover efficiency, which includes rear spillover, scattering, blockage, and ohmic loss efficiency; and $m(e)$ is the wet mapping function: the ratio of the non-hydrostatic constituent of the path delay in the neutral atmosphere at the elevation e to that path delay in the zenith direction. Since the observations were made at different elevation angles down to 10°, decomposition of system temperature according to expression 1 can be easily done using nonlinear least squares. The sky tipping curve analysis procedure of KVN follows the method described in Mangum (2000), Section 6.5.1. We used NMFw wet mapping function (Niell 1996) in our work. Estimates of the opacity, spillover efficiency, and receiver temperature from system temperature measured during observations were within 5%–10% from results derived from tipping curves. Variations of both receiver temperature and opacity varied within 10% over four days. Table 2 shows the average receiver temperature, opacity, and system equivalent flux density (SEFD) in the zenith direction during observations. Using estimates of opacity, we reduced our system temperature to the top of the atmosphere and calibrated fringed amplitudes by multiplying them by a factor $\sqrt{T_{sys,1}\, T_{sys,2}}/G$, where G is the a priori gain.

Since each target source was scheduled in two scans of a three-element interferometer, the self-calibration method for imaging will not work because too few data are available. We computed predicted correlated flux densities for every observation of 14 amplitude calibrator sources using their brightness distributions in the form of CLEAN components from VLBA observations under the Boston University blazar monitoring program. We processed images for epoch 2011 December 2 or 2012 January 27, i.e., within one month from our observations. Using these predicted correlated flux densities, and comparing them with

---

Table 3
The First 8 Rows of the Catalog of Correlated Flux Densities of 637 Sources that Have at Least Three Detections in KVN QCAL-1 Observing Campaign

Source names		Stat.		Correlated flux density			Errors of F_{corr}			Source coordinates	
(1) IAU name	(2) IVS name	(3) Flag	(4) #Det	(5) $F_{<21}$ (Jy)	(6) F_{21-42} (Jy)	(7) $F_{>42}$ (Jy)	(8) $E_{<21}$ (Jy)	(9) E_{21-42} (Jy)	(10) $E_{>42}$ (Jy)	(11) Right ascen (h m s)	(12) Declination ° ′ ″
J0013+4051	0010+405		6	−1.000	−1.000	0.612	−1.000	−1.000	0.018	00 13 31.1302	+40 51 37.144
J0013−0423	0011−046		3	−1.000	−1.000	0.087	−1.000	−1.000	0.014	00 13 54.1309	−04 23 52.294
J0014+6117	0012+610		6	−1.000	−1.000	0.281	−1.000	−1.000	0.016	00 14 48.7921	+61 17 43.542
J0017+8135	0014+813		7	−1.000	0.257	0.254	−1.000	0.016	0.020	00 17 08.4749	+81 35 08.136
J0022+0608	0019+058		6	−1.000	0.449	0.448	−1.000	0.016	0.017	00 22 32.4412	+06 08 04.268
J0027+5958	0024+597		6	−1.000	−1.000	0.189	−1.000	−1.000	0.016	00 27 03.2862	+59 58 52.959
J0029+0554	0027+056		6	−1.000	0.295	0.261	−1.000	0.015	0.015	00 29 45.8963	+05 54 40.712
J0038+1856	0035+186	N	6	−1.000	0.099	0.086	−1.000	0.014	0.015	00 38 28.8915	+18 56 17.641

Notes. Units of right ascension are hours, minutes, and seconds. Units of declination are degrees, minutes, and seconds.

(This table is available in its entirety in machine-readable and Virtual Observatory (VO) forms in the online journal. A portion is shown here for guidance regarding its form and content.)

Table 4
The First 8 Rows of the QCAL-1 Catalog of Positions of 33 Sources Never Before Observed with VLBI

Source Names		J2000 Coordinates		Errors (mas)			Stat	
IAU (1)	IVS (2)	Right Ascension (3)	Declination (4)	$\Delta\alpha$ (5)	$\Delta\delta$ (6)	Corr (7)	No. of Obs (8)	No. of Exp (9)
J0038+1856	0035+186	00 38 28.8915	+18 56 17.641	20.0	13.0	−0.479	6	2
J0202+3943	0159+394	02 02 01.6563	+39 43 21.556	11.0	5.8	−0.235	6	2
J0204+4005	0201+398	02 04 05.1941	+40 05 03.514	20.0	12.0	−0.376	6	2
J0242+2653	0239+266	02 42 20.8303	+26 53 37.722	30.0	17.0	−0.092	4	2
J0251+7226	0246+722	02 51 37.3545	+72 26 55.847	50.0	14.0	−0.287	6	2
J0251+3734	0248+373	02 51 59.1686	+37 34 18.177	33.0	23.0	−0.097	4	2
J0452+1236	0449+125	04 52 42.6001	+12 36 24.586	24.0	18.0	−0.565	5	2
J0502−2057	0500−210	05 02 10.4053	−20 57 16.590	30.0	31.0	−0.615	3	1

Notes. Units of right ascension are hours, minutes, and seconds. Units of declination are degrees, minutes, and seconds.

(This table is available in its entirety in machine-readable and Virtual Observatory (VO) forms in the online journal. A portion is shown here for guidance regarding its form and content.)

the calibrated fringe amplitudes from our observations, we estimated average multiplicative gain factors using least squares. These factors were considered to be constant over each individual observing session. Detailed discussion of this method and approaches for evaluation of errors associated with this method are given in Petrov at al. (2012). Using the same technique, we found that the calibration errors of the QCAL-1 survey were within 15%.

4. QCAL-1 CATALOG

Among 813 observed sources, 799 targets, and 14 calibrators, 637 sources were detected in three or more observations, 27 objects were detected in two observations, 20 objects were detected in only one observation, and 129 objects were not detected at all. If a source had an outlier greater than 0.4 ns in the astrometry solution, we counted that observation as a non-detection. We consider a source reliably detected if it was detected in three or more observations. Since the probability of false detection of an individual observation is 0.01, and considering such events are independent, the probability that all three detections with S/N > 5.4 are spurious is 10^{-6}. The probability that falsely detected observations have residuals less than 0.4 ns for all three observations is 10^{-12} if we regard these cases as statistically independent and 10^{-4} if we regard them as totally dependent.

For each 637 detected sources, we computed the median correlated flux density in three ranges of baseline projection lengths: [0, 21], [21, 42], and [42, 68] megawavelengths, which corresponds to the ranges of 150, 300, and 477 km. The first eight rows of the catalog are presented in Table 3.

Errors in estimates of correlated flux density are determined by two factors: errors in calibration and unaccounted source structure. Since the majority of sources are barely resolved at 43 GHz with the angular resolution of 5 mas that we had in our observations, the first factor dominates. As a test, we analyzed the first and the second observing session separately. The comparison of flux density estimates from independent experiments showed us that they are consistent within 5%–10%. This indicates that our estimate of the calibration uncertainty 15% is close rather to an upper limit of actual errors than the low limit. However, due to the scarceness of redundant observations we have to refrain from attempts to derive more robust statistics of flux density measurements.

In our astrometric solution that used all three observing sessions the following parameters were estimated with least squares: positions of 33 new sources, baseline lengths, and the nuisance parameters, such as clock function and residual atmosphere path delay in zenith direction. We kept positions of remaining 604 sources fixed to their values from the recent update of the Radio Fundamental Catalog that used all available VLBI observations under geodesy and absolute astrometry programs since 1980 April through 2012 June. Positions of these 604 sources defined the orientation of the new catalog of 33 sources.

Table 5
The Minimal Correlated Flux Density in Jy for a Source that Has the
Probabilities of 50%, 70%, 90%, and 95% of Detection in One Observation
During QCAL-1 Campaign

Decl. Range	50%	70%	90%	95%
[−20°, +90°]	75	90	115	130
[−30°, −20°]	105	115	130	140
[−40°, −30°]	140	160	180	190

The first eight entries of the catalog are presented in Table 4. The semimajor axes of the error ellipse from formal uncertainties of source positions are in a range from 8 to 45 mas with the median value of 20 mas. In 2012 March and April, six sources from Table 4 were observed in one scan at 7.9–8.9 GHz with VLBA as fillers under ongoing astrometry project for observations of a complete sample of Two Micron All Sky Survey galaxies (Condon et al. 2011). Uncertainties of source position determined from these observations were in a range of 0.3–3 mas, more than one order of magnitude smaller than in QCAL-1 observations. The average arc length between VLBA and KVN positions is 26 mas, which is consistent with their formal uncertainties.

5. DISCUSSION

Comparing the correlated flux densities and the S/Ns, we can determine for each observations with S/N > 10 the minimal correlated flux density that corresponds to the S/N cutoff equal to 5.4. We built the cumulative distribution of the correlated flux densities that correspond to this cutoff and analyzed them. Sources with low declinations, and we observed sources with declinations as low as −41°, are observed inevitably at low elevations through a thick layer of the atmosphere. This certainly affects our ability to detect a source. Table 5 shows the minimal correlated flux density for a source to be detected over 90 s integration time with a given probability derived from analysis of the cumulative distribution.

The distribution of correlated flux densities from QCAL-1 observations shows a growth of the number of detected sources with decreasing their flux densities until it drops at around 110 mJy (Figure 2). The flux density where the drop begins agrees well with our estimate of the detection limit presented in Table 5.

The distribution does not include other sources from K/Q and Boston University monitoring surveys. At present, we are not in a position to present evidence that the cumulative list of 776 objects from these two surveys and from QCAL-1 is complete at a certain flux density level. More observations and meticulous completeness analysis of the parent source list are needed in order to draw a conclusion about completeness of the Q-band sample. At present, we can firmly say that at least 534 sources have correlated flux densities greater than 200 mJy at projection baseline length of 40 mega wavelengths and 381 objects have correlated flux densities greater than 300 mJy at three-fourths of the celestial sphere with declination >−30 deg.

We can make a coarse estimate of the number of sources with the flux density at Q band greater than 100 mJy. We computed the ratios of Q-band correlated flux density to K-band correlated flux density. For 73% sources the ratio exceeds 0.5 and for 22% it exceeds 1.0. The dependence of the number of sources N at $\delta > -30°$ on the K-band correlated flux density S for $S > 0.35$ Jy is approximated by $N = 182 \cdot S^{-1.279}$, where S is in Jansky. Extrapolating this dependence to flux densities of
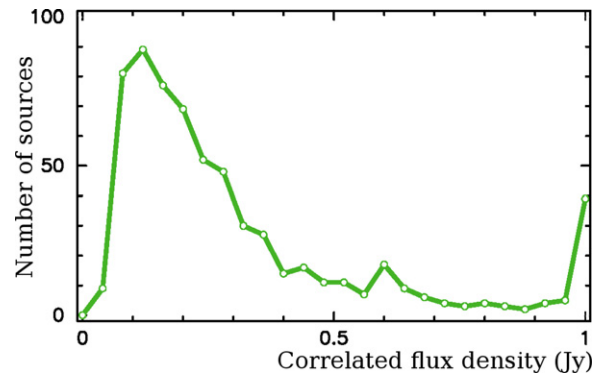

Figure 2. Distribution of the correlated flux densities at baseline projection lengths longer than 21.44 megawavelengths. The last bin of the histogram has all the sources with correlated flux density >1 Jy.
(A color version of this figure is available in the online journal.)

0.2 and 0.1 Jy, we get the expected number of sources: 1426 and 3460, respectively. Considering that 73% sources with K-band correlated flux density >0.2 Jy and 22% sources with K-band correlated flux density in a range of [0.1, 0.2] Jy can be detected in the Q-band with KVN, we get a total expected number of detections: ∼1500 objects.

We selected integration time 90 s for target sources. However, visual inspection of variations of fringe amplitudes with time for strong sources did not show a sign of decorrelation due to either the atmosphere or the frequency standards. We re-ran fringe fitting by dropping cross-correlation samples after 45 and after 60 s since the scan's nominal start. If decorrelation due to phase fluctuations caused by the atmosphere path delay or by the frequency standards is negligible, the S/N grows with an increase of averaging time as a square root of time. Deviation from this dependence in a form of $S/N(t_2) = S/N(t_1) D(t_2) \sqrt{t_2/t_1}$ provides us a measure of decorrelation $D(t)$. We found that the average decorrelation factor is 0.99 when the coherence time is increased from 45 to 60 s and 0.98 when the coherence time is increased from 60 to 90 s. This indicates that the coherence time during the QCAL-1 survey was significantly longer than 90 s.

Considering that (1) 100% of scheduled observations were observed, correlated, and fringe fitted; (2) no noticeable decorrelation due to either frequency standard or atmosphere was found; (3) system temperature was measured for every scan with no abnormalities; (4) receiver temperature showed variations within 10%; (5) the median detection limit was 110 mJy; and (6) positions of new sources were determined with median accuracies of 20 mas, we regard the early science KVN observations for QCAL-1 project as fully successful.

6. SUMMARY

The major result is the catalog of flux densities of 637 compact sources at 43 GHz. Their errors do not exceed 15%. The number of sources detected in Q-band surveys grew by a factor of five and reached 776 objects. An integration time of 90 s allowed us to detect a 115 mJy source at declination >−20° with the probability of 90% in the winter season. We found that our observations were not limited by coherency time of either the atmosphere or the frequency standards. We may tentatively suggest that the coherence time could be increased to 180 s. We can conclude that KVN is able to reliably detect in the Q-band sources with correlated flux densities greater than

100 mJy, at least in winter. More observations are needed in order to judge whether the coherence time during the QCAL-1 campaign was representative.

We observed sources at elevations as low as $10°$ and with declinations as low as $-41°$. The detection limit for sources with declinations below $-30°$ was a factor of 1.5–2 worse than that for sources with declinations greater than $-20°$.

We determined the coordinates of 33 new sources that have not been observed before with VLBI. The median formal position uncertainty from two scans is 20 mas. Comparison of these positions with positions of six sources derived from analysis of VLBA observations at 8 GHz in 2012 confirmed that the formal uncertainties are realistic. Observing sources in 12–15 scans, which requires approximately 30 minutes per source, will bring position uncertainty down to 5–10 mas.

The 56 hr long observing campaign is not sufficient to reach completeness of the AGN population at a certain flux density level. A new campaign, QCAL-2, is planned to achieve this goal. The ongoing KVN K-band calibrator survey (J. A. Lee et al. in preparation) is expected to increase the density of calibrators at 22 GHz for phase referencing observations and it will be used as a pool of targets for QCAL-2.

These early science results met or exceeded our expectations of KVN performance for AGN studies. We conclude that the number of AGNs that KVN is able to detect in the Q band using 1024 Mbps recording rate is well over 1000. These sources can also be used as phase calibrators for observing much weaker targets. With the use of QCAL-1 results, the probability of finding a calibrator for KVN observations within $2°$ of any target is 30%. Future deeper surveys promise to increase this probability significantly and therefore boost our ability to detect interesting targets at high frequencies.

REFERENCES

Beasley, A. J., Gordon, D., Peck, A. B., et al. 2002, ApJS, 141, 13
Condon, J., Darling, J., Kovalev, Y. Y., & Petrov, L. 2011, arXiv:1110.6252
Deller, A., Brisken, W. F., Phillips, C. J., et al. 2011, PASP, 123, 275
Fomalont, E., Petrov, L., McMillan, D. S., Gordon, D., & Ma, C. 2003, AJ, 126, 2562
Han, S.-T., Lee, J.-W., Kang, J., et al. 2008, Int. J. Infrared Milli. Waves, 29, 69
Healey, S. E., Romani, R. W., Cotter, G., et al. 2008, ApJS, 175, 97
Jacobs, C. S., & Sovers, O. J. 2009, in Proc. 19th European VLBI for Geodesy and Astrometry Working Meeting, ed. G. Bourda, P. Charlot, & A. Collioud (Bordeaux: ACSD), 9
Jorstad, S. G., Marscher, A. P., Lister, M. L., et al. 2005, AJ, 130, 1418
Jung, T., Sohn, B. W., Kobayashi, H., et al. 2011, PASJ, 63, 375
Kim, H.-G., Han, S.-T., Sohn, B. W., et al. 2004, in Proc. 7th EVN Symp., ed. R. Bachiller, F. Colomer, J. J. Desmurs, & P. de Vicente (Toledo, OH: OAN), 281
Kovalev, Y. Y., Petrov, L., Fomalont, E., & Gordon, D. 2007, AJ, 133, 1236
Lanyi, G. E., Boboltz, D. A., Charlot, P., et al. 2010, AJ, 139, 1695
Lee, S., Byun, D., Oh, C. S., et al. 2011, PASP, 123, 1398
Mangum, J. G. 2000, Users's Manual for the NRAO 12 m Millimiter-wave Telescope Kitt Peak, Arizona (NRAO; Tucson, AZ: Arizona), http://aro.as.arizona.edu/12m_docs/12m_userman.pdf
Marscher, A. P., Jorstad, S. G., Agudo, I., MacDonald, N. R., & Scott, T. L. 2012, arXiv:1204.6707
Murphy, T., Sadler, E. M., Ekers, R. D., et al. 2010, MNRAS, 420, 2403
Niell, A. E. 1996, J. Geophys. Res., 100, 3227
Petrov, L., Hirota, T., Honma, M., et al. 2007a, AJ, 133, 2487
Petrov, L., Kovalev, Y. Y., Fomalont, E., & Gordon, D. 2005, AJ, 129, 1163
Petrov, L., Kovalev, Y. Y., Fomalont, E., & Gordon, D. 2006, AJ, 131, 1872
Petrov, L., Kovalev, Y. Y., Fomalont, E., & Gordon, D. 2007b, AJ, 136, 580
Petrov, L., Kovalev, Y. Y., Fomalont, E., & Gordon, D. 2011, AJ, 142, 35
Petrov, L. 2012, MNRAS, 416, 1097
Petrov, L., Honma, M., & Shibata, S. M. 2012, AJ, 143, 35
Richards, J. L., Max-Moerbeck, W., Pavlidou, V., et al. 2011, ApJS, 194, 29

---

[8] See http://www.bu.edu/blazars/VLBAproject.html